HHS Public Access

Author manuscript

Exp Eye Res. Author manuscript; available in PMC 2022 July 07.

Published in final edited form as:

Exp Eye Res. 2020 September ; 198: 108135. doi:10.1016/j.exer.2020.108135.

Intravitreal enzyme replacement inhibits progression of retinal degeneration in canine CLN2 neuronal ceroid lipofuscinosis

Rebecca E.H. Whiting[1], **Grace O. Robinson**[1], **Juri Ota-Kuroki**[1], **Stefanie Lim**[1], **Leilani J. Castaner**[1], **Cheryl A. Jensen**[1], **Joseph Kowal**[1], **Annalisa Nguyen**[2], **Carley Corado**[2], **Charles A. O'Neill**[2], **Martin L. Katz**[1]

[1]Neurodegenerative Diseases Research Laboratory, University of Missouri, Columbia, MO 65212, USA

[2]BioMarin Pharmaceutical Inc., 105 Digital Drive, Novato, CA 94949, USA

Abstract

CLN2 neuronal ceroid lipofuscinosis is a rare recessive hereditary retinal and neurodegenerative disease resulting from deleterious sequence variants in *TPP1* that encodes the soluble lysosomal enzyme tripeptidyl peptidase-1 (TPP1). Children with this disorder develop normally, but starting at 2 to 4 years of age begin to exhibit neurological signs and visual deficits. Vision loss that progresses to blindness is associated with progressive retinal degeneration and impairment of retinal function. Similar progressive loss of retinal function and retinal degeneration occur in a dog CLN2 disease model with a *TPP1* null sequence variant. Studies using the dog model were conducted to determine whether intravitreal injection of recombinant human TPP1 (rhTPP1) administered starting after onset of retinal functional impairment could slow or halt the progression of retinal functional decline and degeneration. *TPP1* null dogs received intravitreal injections of rhTPP1 in one eye and vehicle in the other eye beginning at 23.5 to 25 weeks of age followed by second injections at 34–40 weeks in 3 out of 4 dogs. Ophthalmic exams, in vivo ocular imaging, and electroretinography (ERG) were repeated regularly to monitor retinal structure and function. Retinal histology was evaluated in eyes collected from these dogs when they were euthanized at end-stage neurological disease (40–45 weeks of age). Intravitreal rhTPP1 injections were effective in preserving retinal function (as measured with the electroretinogram) and retinal morphology for as long as 4 months after a single treatment. These findings indicate that intravitreal injection of rhTPP1 administered after partial loss of retinal function is an effective treatment for preserving retinal structure and function in canine CLN2 disease.

Keywords

Retinal degeneration; enzyme replacement therapy; genetic diseases; intravitreal drug delivery; neuronal ceroid lipofuscinosis; lysosomal storage disease

Correspondence: Martin L. Katz, University of Missouri School of Medicine, Mason Eye Institute, One Hospital Drive, Columbia, MO 65212, USA; katzm@health.missouri.edu.

1. Introduction

The neuronal ceroid lipofuscinoses (NCLs) are a group of rare hereditary lysosomal storage diseases characterized by progressive neurodegeneration usually accompanied by retinal degeneration and progressive visual impairment (Mole et al., 2011; Weleber, 1998). These disorders result from deleterious sequence variants in one of at least 13 genes (Kousi et al., 2012; Warrier et al., 2013). Among these disorders is CLN2 disease that results from sequence variants in *TPP1*, a gene that encodes the soluble lysosomal enzyme tripeptidyl peptidase-1 (TPP1). Children that are deficient in this enzyme develop normally until the age of 2 to 4 years, at which time they begin to exhibit neurological signs that include impaired speech development, ataxia, seizures, myoclonus, cognitive and motor impairment, and visual failure (Mole et al., 2011). Visual failure is due at least in part to progressive retina degeneration (Weleber, 1998). Over time visual impairment progresses to blindness, and as a result of generalized neurological decline, affected children eventually lose all independent mobility and the ability to communicate. Ultimately the ability to swallow is lost, and many children receive nutritional support using a nasogastric or gastronomy tube. At end-stage disease frequent assisted airway clearance is required to prevent airway blockage. Death due to disease complications usually occurs by the middle teenage years.

A naturally occurring form of CLN2 disease resulting from a null mutation in *TPP1* has been well characterized in a Dachshund model (Awano et al., 2006; Katz et al., 2014; Katz et al., 2015; Sanders et al., 2011; Whiting et al., 2016; Whiting et al., 2014; Whiting et al., 2015). The disease signs and progression are very similar to those in affected children with onset of disease signs beginning at about 4–5 months of age in the dachshunds and proceeding to end-stage disease at about 11 months of age. This makes the CLN2 Dachshund an excellent model for preclinical evaluation of potential therapeutic interventions for this disease. Indeed, we found that periodic infusion of recombinant human TPP1 (rhTPP1) into the cerebrospinal fluid (CSF) of affected dogs resulted in a substantial delay in disease onset and progression and a prolonged healthy lifespan (Katz et al., 2014). These preclinical studies led to the adoption of this treatment for children with CLN2 disease. Children who have been receiving this treatment for over 3 years have exhibited a pronounced therapeutic benefit (Schulz et al., 2018).

In both the dogs and children, CSF infusion of rhTPP1 failed to prevent the progressive vision loss associated with retinal degeneration, apparently because little if any of the rhTPP1 infused into the CSF reached the retina. We have therefore conducted a preclinical study in the Dachshund CLN2 model to determine whether periodic intravitreal injection of rhTPP1 can preserve retinal function and structure. In the dog model, treatments were initiated after some disease-related decline in retinal function had already occurred to evaluate whether treatment with rhTPP1 can halt the progression of existing disease in the retina and maintain remaining retinal function.

2. Materials and methods

2.1. Animals

Dachshunds employed in this study were generated from a research colony maintained in AALAC-accredited facilities at the University of Missouri on a 12:12 daily light cycle. The dogs were socialized daily outside of their kennels. The colony was established in 2002 from a pair of miniature long-haired Dachshunds that were heterozygous for the *TPP1* disease allele. The colony has been maintained continuously since 2002. Affected dogs were generated by breeding *TPP1* disease allele carriers. Periodically carriers from the colony were bred to unrelated homozygous normal Dachshunds to minimize inbreeding.

At approximately 1 week of age the puppies from each litter were implanted with microchips for reliable identification. Cheek swab samples were then obtained from each puppy and used for DNA isolation. The samples were genotyped at the *TPP1* c.325 disease locus using an allelic discrimination assay that distinguishes the normal and disease alleles (Awano et al., 2006). Dogs that were homozygous for the disease allele were enrolled in the study. Some of the carrier dogs were retained for breeding and the remaining dogs were spayed or neutered and adopted out after weaning.

2.2. Treatments

All animals enrolled in the study received oral immunosuppressive therapy (cyclosporine 35 mg BID and leflunomide 10–12 mg SID) starting at approximately 4 months of age, prior to the first intravitreal (IVT) treatment, and continuing throughout the study period. Additional oral anti-inflammatory or immunosuppressive medications, such as prednisone or carprofen were used when necessary. Topical corticosteroid (Durezol; difluprednate QID) and non-steroidal anti-inflammatory (Nevanac; nepafenac TID) drops were administered to the cornea of each eye beginning 24 hours prior to each rhTPP1 dose administration and for at least 1 week post-dose administration. Further administration of topical medications was adjusted based on whether intraocular inflammation occurred; details are provided in the results section.

All animals (Dogs A, B, C, and D) received an initial intravitreal dose of rhTPP1 (0.5 mg) at 23 – 25 weeks of age (approximately 5.5 months), at which time the dogs exhibited deficits in retinal function as assessed by marked declines in ERG b-wave amplitude. A second dose of rhTPP1 (0.25 mg) was scheduled if the b-wave amplitudes on follow-up ERG assessment declined by an amount greater than 20% of the baseline amplitude measurements taken within 1 week prior to the first injection. Dog B was given a second dose 8 weeks following the first dose despite maintenance of ERG amplitudes in order to investigate the effects of redosing. Dog C did not receive a second dose despite ERG declines due to the severity of neurologic disease symptoms at the time a second dose would have been warranted. The dosing regimen for each dog is summarized in Table 1.

Prior to dose administration, each dog was sedated with dexmedetomidine up to 20 μg/kg and buprenorphine (0.015mg/kg) by intramuscular (IM) or intravenous (IV) injection. One drop of topical proparacaine ophthalmic solution and one drop of ofloxacin ophthalmic solution was applied to the left and right eye. The ocular surface was cleaned prior to

dose administration with a dilute (1 in 50) povidone-iodine solution. For each intravitreal injection of TPP1 or vehicle, the dorsolateral bulbar conjunctiva was grasped with forceps and the globe rotated ventromedially. The globe was injected using a 500 μl insulin syringe with a 0.5 inch 28G attached needle at 5–7mm posterior to the limbus with the needle directed posterior to the lens into the mid-vitreous. Following the IVT injection, one drop of ofloxacin ophthalmic solution was applied to the eye and a sub-Tenon's injection of triamcinolone acetonide (2 mg per eye) was performed. After dose administration, dexmedetomidine was reversed using atipamezole (IM) at one-half of the volume of the dexmedetomidine dose.

2.3. Electroretinography

Beginning at 3 months of age, ERG recordings were performed monthly in each dog prior to treatment in order to document typical CLN2 disease-related declines in retinal function at these ages. Baseline measurements were taken within 1 week prior to each intravitreal injection of rhTPP1. ERG recording was repeated every 3 to 4 weeks in the follow-up period after each injection. Bilateral electroretinogram (ERG) evaluations were performed as described previously (Whiting et al., 2013). Scotopic and photopic ERGs were elicited bilaterally and recorded simultaneously with a commercial instrument (HMsERG model 2000; RetVet Corp., Columbia, MO). ERG waveforms in all recordings were evaluated, and the amplitudes for the a- and b-waves were measured as previously described (Whiting et al., 2013). The b-wave amplitudes were compared between the rhTPP1 treated and vehicle control eye for each dog at each time point. Data for each time point was compared to the respective baseline amplitudes collected for each dog prior to treatment and to historical control data collected previously from wild-type dogs and untreated CLN2-affected (*TPP1* −/−) dogs.

2.4. In Vivo Ocular Imaging

Imaging of the retina and vitreous was performed monthly in each dog prior to treatment and was repeated every 3 to 4 weeks in the follow-up period after each injection. Imaging of the was performed with the dog under general anesthesia using a combined confocal scanning laser ophthalmoscope (SLO) and spectral-domain optical coherence tomography (OCT) instrument (Spectralis HRA/OCT, Heidelberg, Germany) as previously described (Katz et al., 2015). Imaging was used to assess and document intraocular inflammation and the development and progression of any disease-related multifocal detachment lesions.

It was not logistically possible to mask which eye was "treated" and which was the control for the in vivo assessments because the same research staff members who performed the treatments also performed the assessments. However, there was almost no risk of bias in acquisition of the ERG and in vivo imaging data. ERG recordings were performed on both eyes simultaneously for each time point, eliminating most possible sources of bias for these data. The retinal imaging was performed using identical procedures for all eyes and time points, so there was minimal chance of bias.

2.5. Ocular Morphology

All four dogs were maintained until they reached neurological end-stage disease when they were 43 to 46 weeks of age (Katz et al., 2014; Tracy et al., 2016). At this point final ERG analysis and ocular imaging were performed. Immediately after imaging while they were still sedated, the dogs were euthanized by intravenous administration of pentobarbital.

Immediately after euthanasia, each eye with approximately 1 cm of the optic nerve attached was enucleated. A 16G needle affixed to a 1 mL syringe was inserted through the cornea into the aqueous chamber and approximately 0.5 mL of aqueous humor was withdrawn and transferred to a cryovial and frozen at −80°C for later analysis. The cornea, iris and lens were then removed from each eye and as much of the vitreous humor as possible was collected, transferred to a cryovial and frozen for later analysis. The remainder of each eye was fixed in 2.5% glutaraldehyde in 0.1 M sodium cacodylate buffer at pH 7.4 (Tracy et al., 2016). After immersing each eyecup in fixative, the optic nerve was cut from the eye, cleaned of adhering tissues, and incubated in the 2.5% glutaraldehyde fixative at room temperature with gentle agitation for at least 24 hours. The fixed tissues were stored in the fixative at room temperature until further dissection could be performed. For histological analyses of the retinas, 8 regions were dissected from along the superior-inferior mid-line each eyecup as illustrated in Figure 1. For optic nerve axon counts, a cross-sectional slice of each optic nerve approximately 1 mm long was cut from the optic nerve and transferred to a separate vial for further processing.

Each of these samples was washed in 0.17 M sodium cacodylate buffer (pH 7.4), post-fixed with osmium tetroxide, and embedded in epoxy resin for light and electron microscopy. Cross-sections of the retina or ciliary body from each region were cut in the orientation shown in Figure 1 on a Reichert Ultracut S ultramicrotome at a thickness of 0.8 μm, mounted on glass slides and stained with toluidine blue. Cross-sections of each optic nerve were obtained mounted in slides and stained in the same manner. Images of each of regions A1, B1, and E1 representing 400 μm of retinal length or 1460 μm of ciliary body length and images of the entire cross section of each optic nerve were obtained with a Leica AF6000 microscope with a computer-controlled motorized stage using a 40 X objective and Leica Application Suite X software to create a composite image of each sample. For regions A and B the number of nuclei in the outer and inner nuclear layers were counted using Photoshop and ImageJ software (https://imagej.nih.gov/ij/) (Katz et al., 2017). Total axon numbers in each optic nerve were determined as described previously (Whiting et al., 2016).

Both image acquisition and quantitative image analyses were performed in a masked manner. The slides were labeled with coded accession numbers prior to image acquisition and given to the staff member who acquired the images. The images were saved in files with the same coded numbers for image analysis. After the quantitative data were obtained, the sample and image identifiers were decoded so that the data could be linked to each individual dog.

For electron microscopy, the blocks used to obtain the sections for light microscopic analysis were trimmed for ultrathin sectioning. Sections of each of these blocks were cut at thickness of 70 to 80 nm and mounted on 200 mesh copper grids. The sections were stained with

lead citrate and uranyl acetate and were examined with a JEOL JEM-1400 transmission electron microscope equipped with a Gatan digital camera. To determine the amount of disease-specific storage material in the retinal ganglion cell bodies of each eye, electron micrographs were obtained of a minimum of 10 ganglion cell bodies from the A1 region of each eye. Using the lasso tool in Adobe Photoshop, the cell body, the nucleus, and each of the cytoplasmic storage bodies were outlined. The Photoshop program calculated the areas of each of these structures. The percent of the cytoplasm occupied by storage bodies in each ganglion cell was then calculated as: Total area storage bodies in the cell/(Area of the cell body – Area of the nucleus). For electron microscopy image acquisition and analyses, the same masking procedure was used as described above the light microscopy analyses.

2.6. Vitreous, Aqueous and Plasma TPP1 Concentrations

Frozen vitreous and aqueous humor samples were shipped on dry ice to BioAgilytix Labs (Durham, NC) for determination of concentrations of rhTPP1. Analyses were performed with a custom enzyme-linked immunosorbent assay (ELISA) using a mouse anti-TPP1 monoclonal antibody for TPP1 capture prepared and characterized by BioMarin Pharmaceutical and a SULFO-TAG- (ruthenium) labeled anti-TPP1 antibody to detect the bound TPP1. The assay was validated by generating standard curves using aqueous and vitreous samples into which specific amounts of purified TPP1 were spiked. Concentrations of TPP1 in the study samples were determined by comparing the ruthenium-specific absorbance to that of the standard curves.

Whole blood was drawn from the jugular or a peripheral vein into lavender-top (EDTA anticoagulant) tubes from each dog at various times during the study. The blood samples were separated by centrifugation and the plasma was collected, transferred to cryovials, and stored frozen at −80°C until thawed for analysis. The plasma samples were shipped on dry ice to Eurofins Pharma Bioanalytics Services US Inc. (St. Charles, MO) for determination of plasma TPP1 concentrations. Analyses were performed using an ELISA assay that employed the same anti-TPP1 antibody as was used for the vitreous and aqueous humor assays. Standards (STD) were prepared by spiking TPP1 into pooled 100% canine K_2EDTA plasma from normal healthy dogs. Blank, standard, and study samples were added to a multiwell plate coated with a mouse anti-TPP1 monoclonal antibody. After capture of TPP1 to the immobilized antibody, unbound materials were removed by a wash step, followed by addition of and incubation with affinity-purified rabbit anti-TPP1 polyclonal antibody to detect bound TPP1. Following an additional wash step, horseradish peroxidase (HRP)-conjugated goat anti-rabbit polyclonal antibody solution was added to each well. After a final wash step, a tetramethylbenzidine (TMB) peroxide substrate solution was added to produce colorimetric signal, which was proportional to the amount of TPP1 bound by the capture reagent. The color development was stopped after an incubation period of 10–15 minutes, by addition of 2N sulfuric acid (H_2SO_4), and the optical density (OD) signal was measured at 450 nm with reference to 650 nm.

2.7. Plasma Anti-TPP1 Antibody Determinations

Frozen blood plasma samples collected and stored as described above were shipped on dry ice to ICON Laboratory Services, Inc. (Whitesboro, NY) for determination of plasma

concentrations of anti-TPP1 antibodies using an electrochemiluninescent (ECL) assay. Samples (including positive controls and pooled negative control) are diluted 1:10 in Diluent Buffer and loaded into the appropriate wells of a polypropylene plate. Alternatively, samples may be diluted directly in the wells of a polypropylene transfer plate. The samples are then diluted 1:3 by the addition of a 3X Master Mix (an equal concentration of Ruthenylated (Sulfo-tagged) TPP1 and Biotinylated TPP1 labels prepared in diluent buffer) to the samples in the wells of a polypropylene plate. This dilutes the Master Mix and the samples to 9 and results in a final plasma concentration of 3.33%. Samples are incubated on the transfer plate for approximately one hour protected from light. Detection of anti-TPP1 antibodies is based on the bivalent characteristics of the antibody. During this incubation, anti-TPP1 antibodies will bind to both the Sulfo-tagged and Biotinylated rhTPP1 molecules to form an antibody complex bridge. Samples are then dispensed from the transfer plate onto a streptavidin coated assay plate that has been blocked for at least one hour. Samples are incubated on the streptavidin coated assay plate for approximately one hour protected from light. The Biotinylated TPP1 in the complex will bind to the streptavidin in the wells, allowing unbound material to be washed away. Only the samples that contain antibody bound to both the Biotinylated TPP1 and the Sulfo-tagged TPP1 will generate an ECL signal. The plate is then washed and a tripropylamine (TPA)-containing Read Buffer is added to the plate. In the presence of TPA, ruthenium produces a chemiluminescent signal that is triggered when voltage is applied. The signal produced is proportional to the amount of TPP1 antibody present.

2.8. Statistical Analyses

Because each of the dogs was subjected to a different treatment regimen, most data from the 4 dogs were not pooled for statistical analysis. An exception was analysis of the data on cell densities in the inner and outer nuclear layers of the retinas collected at the time of euthanasia. For both cell layers the data were not normally distributed, so comparisons between the treated and control eyes was performed using the Mann-Whitney Rank Sum Test. A second exception was comparison of the numbers of axons in the optic nerves of the treated and control eyes. In this case the data were normally distributed, so the comparison between treated and control eyes was performed using Student’s t-test. All statistical tests were performed using SigmaPlot (Systat Software Inc., San Jose, CA).

3. Results

3.1. TPP1 Concentrations in Aqueous Humor, Vitreous Humor and Plasma

None of the vehicle-treated eyes had detectable levels of TPP1 in the aqueous humor. Measurable amounts of TPP1 were present in the aqueous humor of TPP1-treated eyes of 3 of the 4 dogs in this study (Table 2). A substantial amount of TPP1 was present in the aqueous in dog A that was euthanized one day after the last IVT injection. In eyes injected at longer intervals before euthanasia and sample collection, the aqueous levels of TPP1 were near or below the limit of quantitation.

None of the vehicle-treated eyes had detectable levels of TPP1 in the vitreous with the exception of dog A in which the control eye had 14.6 ng/mL of TPP1. At the same time

the TPP1 concentration in the vitreous of the TPP1-treated eye was 62,365 ng/mL (Table 2). This indicates that a very small amount of TPP1 appears to get from the treated eye to the contralateral eye shortly after injection.

Plasma TPP1 concentrations were determined in samples obtained at times ranging from 1 to 140 days after the first or second IVT injections. In none of the samples was the plasma concentration above the limit of quantitation (1.25 ng/mL). In an additional affected dog, plasma samples were analyzed for TPP1 concentrations at 1, 3, 6, 24, 48 and 96 hours after an IVT injection of 1 mg rhTPP1. Barely detectable concentrations of TPP1 were only observed at the 6, 24 and 48 hour time points, peaking at 3.36 ng/mL at 24 post-injection.

3.2. Plasma Antibody-rhTPP1 Titers

Intravitreal injection of rhTPP1 resulted in a robust systemic immune response to TPP1 as indicated by the presence of anti-TPP1 antibodies in the blood plasma of the treated dogs. In plasma samples obtained prior to the first rhTPP1 injection, no anti-TPP1 antibodies could be detected in any of the dogs. Dog C, which received a single injection of 0.5 mg TPP1 at 25 weeks of age, had a modest antibody titer at 140 post-injection (Table 3). The remaining dogs received two IVT injections of rhTPP1, 0.5 mg at 23.5 to 25 weeks of age and 0.25 mg at 33.5 to 39.5 weeks of age (Table 1). At 67 and 48 weeks after the second injections, dogs B and D had very high antibody titers (Table 2). Dog A had to be euthanized one day after the second IVT injection. At this time, antibody titer was minimal (Table 3). This suggests that at the time this plasma was obtained, the dog had not yet mounted a full immune response to the second injection. The sample obtained for antibody titer determination in dog A was obtained 140 days after the first IVT injection.

3.3. Neurological disease progression

Starting at 20 weeks of age, the dogs were each assessed weekly with an established panel of phenotypic neurological markers of disease progression (Katz et al., 2014; Katz et al., 2015). Based on these assessments, in dogs that underwent the IVT treatments the neurological disease progression unrelated to visual function was not altered relative to that of untreated affected dogs that were evaluated previously (Katz et al., 2014; Katz et al., 2015). All four dogs reached the established criterion for end-stage disease at which euthanasia was performed between 40 and 45 weeks of age.

3.4. In vivo retinal imaging

All dogs retained normal fundus images in both eyes during the period following the initial dose. The day following the second dose, dogs B and D exhibited mild intraocular inflammation, and in both cases the active inflammation had resolved by 3–4 weeks post injection. However, vitreal opacity persisted through the remainder of the study in both dogs, though to a greater degree in dog B than in dog D (Figure 2).

Dog C developed widespread canine multifocal retinopathy (CMR) lesions in the control eye while these lesions were completely prevented in the treated eye that received only a single injection at 25 weeks of age. CMR lesions are associated with canine CLN2 disease (Whiting et al 2015) with a variable age of onset, though when they occur progression is

bilaterally symmetrical. The other 3 dogs (A, B, D) did not develop significant CMR lesions in either eye during the study period.

3.5. Electroretinography

Following the initial dose of rhTPP1, no significant declines in b-wave amplitude were observed in any of the dogs for at least 12 weeks (Figures 3–5). Dog A exhibited a 20% reduction in amplitudes 15.5 weeks after the initial dose, and a second dose was administered. Following the second dose, a neurologic episode unrelated to dose administration occurred and necessitated humane euthanasia which prevented follow-up ERG recordings after the second dose for Dog A. Though b-wave amplitudes in Dog B remained at baseline levels, a second dose was administered 8 weeks following the initial dose to investigate the effects of redosing. Following the second dose, Dog B exhibited a slight increase in b-wave amplitude, and amplitudes were similar to baseline #1 measurements for the remainder of the study period. Dogs C and D exhibited more than 20% decline in b-wave amplitude 12–13 weeks after the initial dose. Dog C was not re-dosed due to the severity of disease-related neurologic symptoms at this time. While amplitudes declined further for the next 2 months in Dog C, the final ERG measurements were similar to baseline measurements. Dog D exhibited marked intraocular inflammation after the second dose, which resulted in significant decline in ERG b-wave amplitudes. However, once the inflammation had resolved, ERG amplitudes returned tothe same level as baseline values recorded immediately prior to the second dose (Figures 3–6).

3.6. Assessment of retinal cell numbers at end-stage disease

IVT administration of rhTPP1 was effective in inhibiting disease-related cell losses from both the inner and outer nuclear layers (INL and ONL) of the retinas (Figures 7 and 8). Although there was some variability between dogs in cell numbers for each region analyzed, in almost every region for each of the dogs, the cell densities were higher in the rhTPP1treated eye than the vehicle-treated eye. The only exception was the mid-superior region of the retina of dog A (Figure 7). When the data were pooled for the four dogs, for each region of the eyes there were significantly more cells in both the INL and ONL of the rhTPP1-treated eyes than in the vehicle-treated eyes ($p<0.05$, Mann-Whitney Rank Sum Test).

Since each retinal ganglion cell has one axon that traverses the optic nerve, the numbers of intact ganglion cells in each eye was determined indirectly by counting the numbers of axons in stained cross-sections of the optic nerve from each eye. A representative image of an optic nerve section used for these analyses is shown in Figure 9. Dog B had the same number of axons in the optic nerves of both eyes (Table 4). In each of the other dogs there were fewer axons in the optic nerve of the vehicle-treated eye than in the eye treated with rhTPP1 (Table 4). The difference in axon numbers between the rhTPP1-treated and control eyes was not statistically significant ($p=0.07$, t-test), but the power of the statistical comparison with alpha = 0.05 was only 0.36, so the data are not sufficient to rule out that rhTPP1 treatment was effective in inhibiting disease-related loss of ganglion cells (or at least of their axons).

3.7. Assessment of retinal ganglion cell storage body content at end-stage disease

Canine CLN2 disease is characterized by an abundant accumulation of lysosomal storage bodies in the retinal ganglion cells (Whiting et al., 2015). To determine whether IVT rhTPP1 treatment was effective in ameliorating this accumulation, the fraction the cytoplasmic area composed of storage bodies was assessed in thin sections of the central retina from each eye of each dog. At end-stage disease the ganglion cell storage body content of the rhTPP1-treated eyes was an average of only 12% of that of the vehicle-treated eyes (Table 5). The storage bodies were dramatically smaller and fewer in number in the rhTPP1-treated eyes than in the vehicle treated eyes (Figure 10).

3.8. Assessment of other aspects of retinal morphology at end-stage disease

In the rhTPP1-treated eyes, the ultrastructure of the rod outer segments of the central retina was relatively normal and the distal ends of the outer segments were closely apposed to the apical side of the retinal pigment epithelium (RPE) (Figure 11C). In contrast, in the vehicle-treated eyes, there was a gap between the ends of most of the rod outer segments and the apical surface of the RPE, and only a fraction of the outer segments extended to the RPE apical surface. Of those that did, the apical ends of the outer segments exhibited an abnormal arrangement of the disc membranes (Figure 11A), suggestive of a defect in outer segment disc shedding and phagocytosis by the RPE (Behbehani et al., 1984; LaVail, 1983; Matthes and LaVail, 1989). In the vehicle treated eyes, the many shorter than normal rod outer segments exhibited an abnormal irregularity in disc electron density and were unsheathed by long thin RPE apical processes (Figure 11B).

In the vehicle-treated retinas the axons of the biopolar cells in the outer plexiform layer almost always terminated at the level of the inner-most nuclei of the ONLor even further from the ONL(Figure 12A). The axons seldom penetrated into the ONL. In contrast, in the rhTPP1-treated eyes the majority of the bipolar cells extended between photoreceptor cell nuclei into the ONL(Figure 12B).

In the rhTPP1-treated eyes, the stroma of the ciliary bodies underlying the pigmented epithelium was tightly compact throughout the tissue (Figure 13B). In contrast, in the vehicle-treated eyes, the ciliary bodies were thicker, and the stroma was more loosely organized with acellular gaps in the tissue (Figure 13A).

Perivascular cuffing indicative of inflammation was observed around blood vessels in the retinal ganglion cell/nerve fiber layer in some of the rhTPP1-treated eyes (Figure 14). When present, the degree of perivascular cuffing was more pronounced in the mid-peripheral retina than in the central retina. No such cuffing was noted in any of the vehicle-treated eyes. The mass of cells that surround blood vessels in perivascular cuffs typically consist of lymphocytes or plasma cells and are indicative of inflammation often associated with an immune reaction. The fact that this cuffing was only observed in the rhTPP1-treated eyes suggests that it is the result of an immune reaction to the rhTPP1.

The degree of perivascular cuffing correlated with the time between the last rhTPP1 injection and euthanasia (Table 6). No cuffing was present in the treated retina of dog C who received a single injection of 0.5 mg of rhTPP1 at 25 weeks of age and was euthanized

at 44.5 weeks of age. Likewise, perivascular cuffing was not observed in the treated eye of dog A, who also received an injection of 0.5 mg of rhTPP1 at 25 weeks and then a second injection of 0.25 mg of rhTPP1 just prior to euthanasia at 40 weeks of age. On the other hand, both dogs B and D exhibited significant perivascular cuffing around the inner retinal vessels of the rhTPP1-treated eyes, with the cuffing being more pronounced in dog B. Both dogs were treated with 0.5 mg rhTPP1 at 25 weeks of age. Dog D received a subsequent injection of 0.25 mg rhTPP1 at 38 weeks of age and was euthanized 4 weeks later, and dog B received an injection of 0.25 mg rhTPP1 at 42 weeks of age and was euthanized one week later. These data suggest that the inflammation indicated by the perivascular cuffing around inner retinal vessels subsided over time after administration of rhTPP1. This is consistent with the clinical observations of inflammation noted in the ophthalmic examinations of these dogs.

4. Discussion

These studies demonstrate that intravitreal administration of rhTPP1 was quite effective in preserving retinal function and structure in dogs with CLN2 disease, even when the treatment was initiated after the onset of decline in retinal function as assessed with the ERG. Children with CLN2 disease that are currently receiving rhTPP1 CNS enzyme replacement therapy must undergo four-hour intracerbroventricular (ICV) infusions every other week for life (Schulz et al., 2018). Potential complications of this treatment are minimized by the fact that the ICV infusions are administered through a subcutaneous port connected to an implanted catheter. Intravitreal administration, on the other hand, must be done by injection into the eye. Frequent intravitreal injections are associated with risks of complications (Baudin et al., 2018; Berger et al., 2019; Kotlyar et al., 2019; Shin et al., 2018). It is therefore quite encouraging that a single intravitreal injection of rhTPP1 in a 25-week old dog (Dog C) was effective in preserving retinal function and structure to end-stage disease at 45 weeks of age. In Dog C, there was essentially no declinein ERG b-wave amplitudes between the time of the single injection and euthanasia, indicating that the treatment effect lasted at least this long. Because the dogs succumbed to the neurological disease at 40 to 45 weeks of age, we were unable to determine the maximum duration of the treatment effect.

The reason for the long-lasting therapeutic benefit of a single rhTPP1 injection is not apparent. One possibility is that the rhTPP1 has a long residence in the retinal tissues. Although the concentration of the injected protein in the vitreous was quite high at one day post-injection, it was undetectable in the vitreous at subsequent time points as early as 58 days after administration (Table 2). In the aqueous on the other hand, rhTPP1 could be detected as long as 140 days after a single injection (Table 2). Due to limited samples, we were not able to determine the amounts of TPP1 in the retinas at the time of euthanasia. Another possible explanation for the long duration of the therapeutic benefit is that it is the result of a reversal of the accumulation of lysosomal storage bodies in the retina. Indeed, we found a reduction of retinal ganglion cell storage body content by 76% to over 90% in the treated eye compared to the control eye of each dog. This would suggest that the presence of large amounts of storage material within a cell may be detrimental and that prevention of this accumulation can preserve normal retinal structure and function. The mechanisms

by which accumulated storage material could exert adverse effects on cells is unknown for CLN2 disease and most other lysosomal storage diseases.

Although only 4 dogs were evaluated in this study, the treatment effect was sufficiently robust to demonstrate clear treatment effects with this number of dogs. In a previous study, treating the same number of dogs with intracerebroventricular infusion of rhTPP1 was sufficient to enable regulatory approval for human clinical trials of this treatment (Katz et al., 2014; Schulz et al., 2018). Federal policies on the use of animals in research require that the number of animals used be the minimum necessary. This is particularly important when species such as dogs that are kept as pets are employed.

Some of abnormalities that were observed with electron microscopy only in the control eyes, such as shortening of axons in the outer plexiform layer, were not quantified. However all of the interpretation of ultrastructural features as being abnormal was based on differences not only between the treated and control eyes, but also between the control eyes and the well-documented ultrastructure of the normal canine retina. Based on these comparisons, we are confident that ultrastructural differences between the treated and control eyes are treatment-related. This is supported by the fact that these differences are consistent with the differences in ERG responses.

The only complication of the treatments was transient intraocular inflammation after the second rhTPP1 injections in two of the dogs (dogs B and D). This inflammation was likely mediated by a systemic immune reaction to the rhTPP1 since both of these dogs and neither the dog that received a single rhTTP1 injection nor the dog that was euthanized shortly after the second injection exhibited the inflammatory response. The dogs that received two rhTPP1 injections also had very high plasma anti-TPP1 antibody titers, indicating that these dogs had mounted a systemic immune response to the injected protein (Table 3). Plasma anti-TPP1 antibody titers were low in the dog that received a single rhTPP1 injection suggesting that the first injection primed the immune system to respond to the subsequent exposure to rhTPP1. In addition, the inflammatory response was observed only in the eyes treated with rhTPP1 and not in the contralateral eyes injected with vehicle (Figure 2). This suggests a direct immune response to the recombinant protein and that the intraocular inflammation was immune-mediated. The inflammation was likely due, at least in part, to rhTPP1 within the retina, since in the affected eyes there was perivascular cuffing around the retinal vessels indicating a migration of inflammatory cells into the retina (Figure 14). Although the intraocular inflammation was an adverse reaction, it did not interfere with the therapeutic benefit on the ERG except transiently in Dog D. Other studies have similarly observed recovery of the ERG and visual acuity after resolution of an inflammatory episode (Chong et al., 2010; Cukras et al., 2018), which is encouraging and supports the idea that transient inflammation does not appear to cause long-term damage to the retina. Intraocular inflammation was associated with long-term vitreal clouding. The mechanism for this is not apparent. The immunosuppressant treatments that were administered to the dogs were not effective in preventing the rhTPP1-mediated inflammation. Further research will be necessary to elucidate the mechanisms that underlie the intraocular inflammation.

Although the possibility of intraocular inflammation secondary to IVT administration is of concern, previous studies and currently used treatments for eye disorders suggest that this complication is less likely to occur in human subjects than in dogs. Treatment-related observed in preclinical studies using IVT administration of heterologous protein are well known (Krzystolik et al., 2002). These inflammatory complications have not occurred in humans treated with a variety of approved drugs administered via intravitreal injection (Wakshull et al., 2017). Frequent long-term IVT administration of recombinant antibody fragments has been employed for years in treating age-related macular degeneration and other retinal disorders with minimal inflammatory complications (Poku et al., 2014). These observations suggest that IVT injection of rhTPP1 in children with CLN2 disease is unlikely to result in significant intraocular inflammation. However, if this complication does occur, the intraocular inflammation can be effectively treated with immunosuppressants (Bae and Lee, 2010; Bakri et al., 2008; Wickremasinghe et al., 2008).

In a recent similar study, we found that initiating IVT injections of rhTPP1 to *TPP1−/−* dogs prior to the onset of clinical signs was effective in delaying both the onset and the progression of retinal degenerative changes (Whiting et al., 2020). The latter study provided a good proof of principle for rhTPP1 enzyme replacement therapy for the retina in CLN2 disease. However, this disorder is rarely diagnosed in children prior to the onset of vision loss. Thus, the current study in which treatment was initiated after the onset of clinical signs is more relevant to practical human application.

The treatment described in this study may be an effective adjunct to ICV infusion of rhTPP1 that has been shown to be effective in preserving CNS structure and function in the Dachshund CLN2 disease model (Katz et al., 2014). The CNS treatment did not preserve retinal structure or function in this model (Whiting et al., 2014), presumably because little if any of the rhTPP1 infused into the CSF reaches the retina beyond possibly the retinal ganglion cells. It appears likely that combined ICV and IVT administration would inhibit disease-related pathology of both the CNS and retina. However, a combined treatment regimen could be accompanied by more severe intraocular inflammation than was observed in this study. Further investigation will be necessary to determine the safety and efficacy of combined CNS and retinal therapy.

Acknowledgements

We thank those who contributed to the care and health of the dogs and colony management, Drs. Dawna Voelkl and Dietrich Volkmann who performed and organized the dog breeding procedures, Jeffrey Student for technical assistance, and the students that socialize the dogs daily and assist with procedures. Supported in part by U.S. National Institutes of Health grant EY023968.

References

Awano T, Katz ML, O'Brien DP, Sohar I, Lobel P, Coates JR, Khan S, Johnson GC, Giger U, Johnson GS, 2006. A frame shift mutation in canine TPP1 (the ortholog of human CLN2) in a juvenile Dachshund with neuronal ceroid lipofuscinosis. Mol Genet Metab 89, 254–260. [PubMed: 16621647]

Bae JH, Lee SC, 2010. Bilateral intraocular inflammation after intravitreal bevacizumab in Behcet's disease. Eye 24, 735. [PubMed: 19543240]

Bakri SJ, Larson TA, Edwards AO, 2008. Intraocular inflammation following intravitreal injection of bevacizumab. Graefes Arch Clin Exp Ophthalmol 246, 779–781. [PubMed: 18204851]

Baudin F, Benzenine E, Mariet AS, Bron AM, Daien V, Korobelnik JF, Quantin C, Creuzot-Garcher C, 2018. Association of Acute Endophthalmitis With Intravitreal Injections of Corticosteroids or Anti-Vascular Growth Factor Agents in a Nationwide Study in France. JAMA Ophthalmol 136, 1352–1358. [PubMed: 30242325]

Behbehani MM, Bowyer DW, Ruffolo JJ, Kranias G, 1984. Preservation of retinal function in the RCS rat by laser treatment. Retina 4, 257–263. [PubMed: 6531522]

Berger V, Munk MR, Lersch F, Wolf S, Ebneter A, Zinkernagel MS, 2019. Association of Intravitreal Injections With Blood Pressure Increase: The Following Excitement and Anxiety Response Under Intravitreal Injection Study. JAMA Ophthalmol 137, 87–90. [PubMed: 30383158]

Chong DY, Anand R, Williams PD, Qureshi JA, Callanan DG, 2010. Characterization of sterile intraocular inflammatory responses after intravitreal bevacizumab injection. Retina 30, 1432–1440. [PubMed: 20559156]

Cukras C, Wiley HE, Jeffrey BG, Sen HN, Turriff A, Zeng Y, Vijayasarathy C, Marangoni D, Ziccardi L, Kjellstrom S, Park TK, Hiriyanna S, Wright JF, Colosi P, Wu Z, Bush RA, Wei LL, Sieving PA, 2018. Retinal AAV8-RS1 Gene Therapy for X-Linked Retinoschisis: Initial Findings from a Phase I/IIa Trial by Intravitreal Delivery. Mol Ther 26, 2282–2294. [PubMed: 30196853]

Katz ML, Coates JR, Sibigtroth CM, Taylor JD, Carpentier M, Young WM, Wininger FA, Kennedy D, Vuillemenot BR, O'Neill CA, 2014. Enzyme replacement therapy attenuates disease progression in a canine model of late-infantile neuronal ceroid lipofuscinosis (CLN2 disease). J Neurosci Res 92, 1591–1598. [PubMed: 24938720]

Katz ML, Jensen CA, Student JT, Johnson GC, Coates JR, 2017. Cervical spinal cord and motor unit pathology in a canine model of SOD1-associated amyotrophic lateral sclerosis. J Neurol Sci 378, 193–203. [PubMed: 28566164]

Katz ML, Tecedor L, Chen Y, Williamson BG, Lysenko E, Wininger FA, Young WM, Johnson GC, Whiting RE, Coates JR, Davidson BL, 2015. AAV gene transfer delays disease onset in a TPP1-deficient canine model of the late infantile form of Batten disease. Sci Transl Med 7, 313ra180.

Kotlyar B, Shapiro M, Blair M, 2019. Exudative Retinal Detachment Following Intravitreal Chemotherapeutic Treatment for Retinoblastoma. Ophthalmic Surg Lasers Imaging Retina 50, 248–252. [PubMed: 30998248]

Kousi M, Lehesjoki AE, Mole SE, 2012. Update of the mutation spectrum and clinical correlations of over 360 mutations in eight genes that underlie the neuronal ceroid lipofuscinoses. Hum Mutat 33, 42–63. [PubMed: 21990111]

Krzystolik MG, Afshari MA, Adamis AP, Gaudreault J, Gragoudas ES, Michaud NA, Li W, Connolly E, O'Neill CA, Miller JW, 2002. Prevention of experimental choroidal neovascularization with intravitreal anti-vascular endothelial growth factor antibody fragment. Arch Ophthalmol 120, 338–346. [PubMed: 11879138]

LaVail MM, 1983. Outer segment disc shedding and phagocytosis in the outer retina. Trans Ophthalmol Soc U K 103, 397–404. [PubMed: 6380008]

Matthes MT, LaVail MM, 1989. Inherited retinal dystrophy in the RCS rat: composition of the outer segment debris zone. Prog Clin Biol Res 314, 315–330. [PubMed: 2608665]

Mole SE, Williams R, Goeble HH, 2011. The Neuronal Ceroid Lipofuscinoses (Batten Disease), 2nd ed. Oxford University Press.

Poku E, Rathbone J, Wong R, Everson-Hock E, Essat M, Pandor A, Wailoo A, 2014. The safety of intravitreal bevacizumab monotherapy in adult ophthalmic conditions: systematic review. BMJ Open 4, e005244.

Sanders DN, Kanazono S, Wininger FA, Whiting RE, Flournoy CA, Coates JR, Castaner LJ, O'Brien DP, Katz ML, 2011. A reversal learning task detects cognitive deficits in a Dachshund model of late-infantile neuronal ceroid lipofuscinosis. Genes Brain Behav 10, 798–804. [PubMed: 21745338]

Schulz A, Ajayi T, Specchio N, de Los Reyes E, Gissen P, Ballon D, Dyke JP, Cahan H, Slasor P, Jacoby D, Kohlschutter A, Group CLNS, 2018. Study of Intraventricular Cerliponase Alfa for CLN2 Disease. N Engl J Med 378, 1898–1907. [PubMed: 29688815]

Shin YI, Sung JY, Sagong M, Lee YH, Jo YJ, Kim JY, 2018. Risk factors for breakthrough vitreous hemorrhage after intravitreal anti-VEGF injection in age-related macular degeneration with submacular hemorrhage. Sci 8, 10560.

Tracy CJ, Whiting RE, Pearce JW, Williamson BG, Vansteenkiste DP, Gillespie LE, Castaner LJ, Bryan JN, Coates JR, Jensen CA, Katz ML, 2016. Intravitreal implantation of TPP1-transduced stem cells delays retinal degeneration in canine CLN2 neuronal ceroid lipofuscinosis. Exp Eye Res 152, 77–87. [PubMed: 27637672]

Wakshull E, Quarmby V, Mahler HC, Rivers H, Jere D, Ramos M, Szczesny P, Bechtold-Peters K, Masli S, Gupta S, 2017. Advancements in Understanding Immunogenicity of Biotherapeutics in the Intraocular Space. Aaps J 19, 1656–1668. [PubMed: 28795351]

Warrier V, Vieira M, Mole SE, 2013. Genetic basis and phenotypic correlations of the neuronal ceroid lipofusinoses. Biochim Biophys Acta 1832, 1827–1830. [PubMed: 23542453]

Weleber RG, 1998. The dystrophic retina in multisystem disorders: the electroretinogram in neuronal ceroid lipofuscinoses. Eye 12, 580–590. [PubMed: 9775220]

Whiting RE, Jensen CA, Pearce JW, Gillespie LE, Bristow DE, Katz ML, 2016. Intracerebroventricular gene therapy that delays neurological disease progression is associated with selective preservation of retinal ganglion cells in a canine model of CLN2 disease. Exp Eye Res 146, 276–282. [PubMed: 27039708]

Whiting RE, Narfstrom K, Yao G, Pearce JW, Coates JR, Castaner LJ, Jensen CA, Dougherty BN, Vuillemenot BR, Kennedy D, O'Neill CA, Katz ML, 2014. Enzyme replacement therapy delays pupillary light reflex deficits in a canine model of late infantile neuronal ceroid lipofuscinosis. Exp Eye Res 125, 164–172. [PubMed: 24954537]

Whiting RE, Narfstrom K, Yao G, Pearce JW, Coates JR, Castaner LJ, Katz ML, 2013. Pupillary light reflex deficits in a canine model of late infantile neuronal ceroid lipofuscinosis. Exp Eye Res 116, 402–410. [PubMed: 24135299]

Whiting RE, Pearce JW, Castaner LJ, Jensen CA, Katz RJ, Gilliam DH, Katz ML, 2015. Multifocal retinopathy in Dachshunds with CLN2 neuronal ceroid lipofuscinosis. Exp Eye Res 134, 123–132. [PubMed: 25697710]

Whiting REH, Jacqueline W Pearce JW, Daniella P Vansteenkiste DP, Bibi K, Stefanie Lim S, Kick GOR, Castaner LJ, Sinclair J, Chandra S, Nguyen A, O'Neill CA, Katz ML, 2020. Intravitreal enzyme replacement preserves retinal structure and function in canine CLN2 neuronal ceroid lipofuscinosis. Exp Eye Res In press.

Wickremasinghe SS, Michalova K, Gilhotra J, Guymer RH, Harper CA, Wong TY, Qureshi S, 2008. Acute intraocular inflammation after intravitreous injections of bevacizumab for treatment of neovascular age-related macular degeneration. Ophthalmology 115, 1911–1915. [PubMed: 18672291]

Highlights

- Progressive retinal degeneration occurs in canine CLN2 neuronal ceroid lipofuscinosis.
- Retinal degeneration results from deficiency in the lysosomal enzyme TPP1.
- Intravitreal injection of recombinant TPP1 after onset of retinal degeneration inhibits further declines in retinal structure and function.

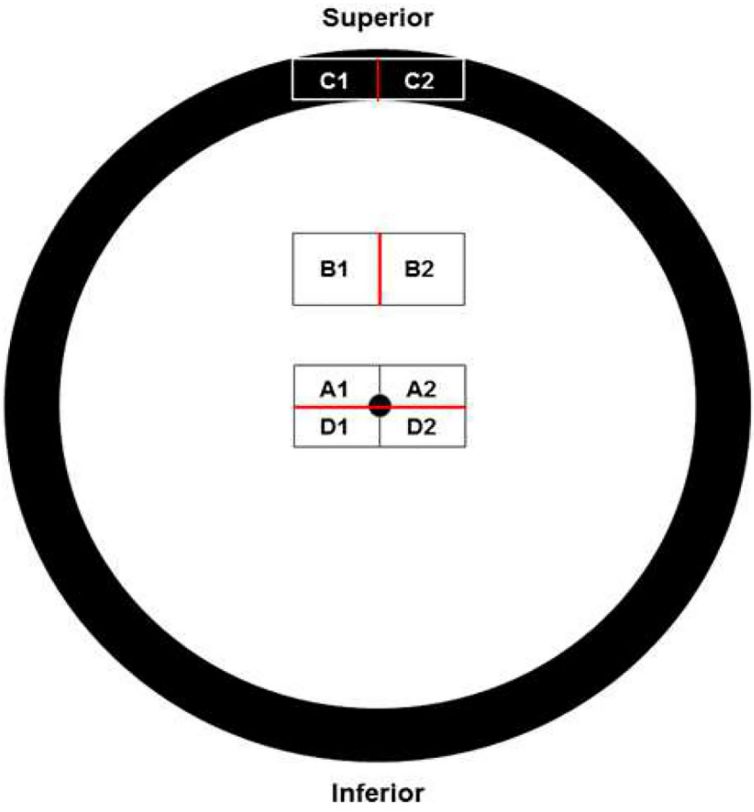

Figure 1.

Diagram illustrating the locations in the eyes from which areas were dissected for morphological analyses. Red lines indicate the edges from each area from which sections were cut. Regions A1, A2, D1, and D2 are from the area of the retina centered on the optic nerve head (black dot in center of diagram). Areas B1 and B2 were mid-way between the optic nerve head and the superior peripheral edge of the retina. Areas C1 and C2 included the ora serrata and the base of the iris.

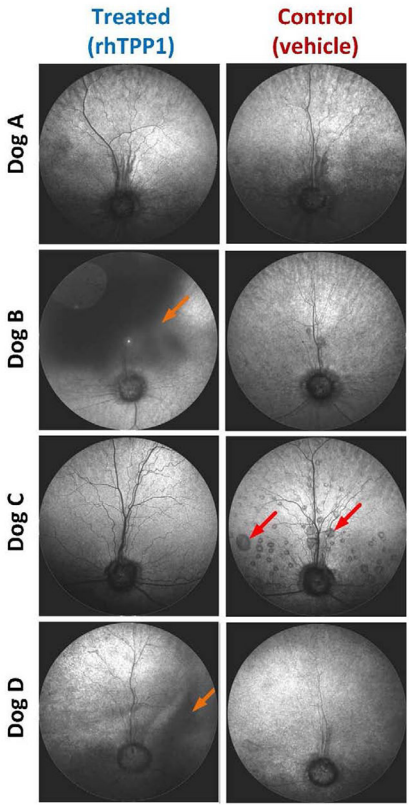

Figure 2.

Scanning laser ophthalmoscopic (SLO) fundus images from all dogs at the end of the study. Images remained normal in all dogs following the initial dose, but dogs B and D exhibited intraocular inflammation following the second dose. While active inflammation gradually resolved, vitreal opacity persisted through the remainder of the study in both dogs (orange arrows). Final images for dog A were taken days prior to the second dose; follow-up images were not possible due to unscheduled euthanasia. Dog C exhibited widespread serous retinal detachments in the control eye such as those indicated by red arrows, while none were noted in the treated eye.

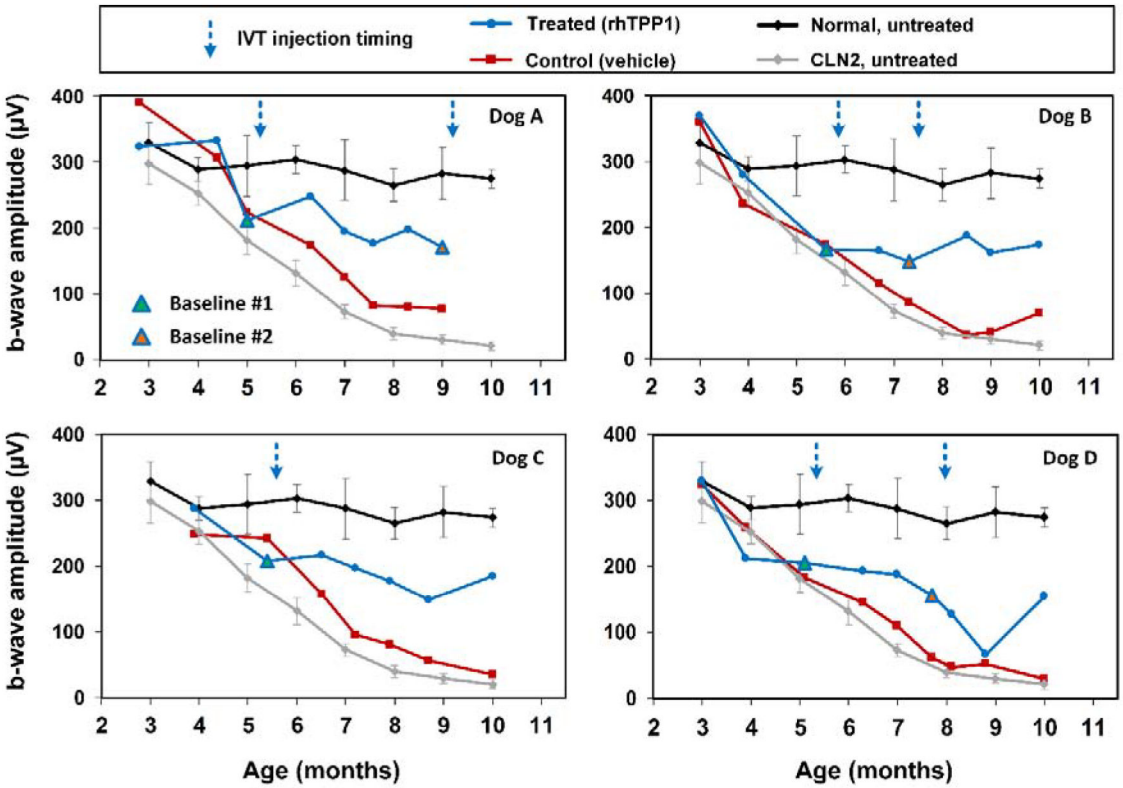

Figure 3.

Post symptomatic intravitreal rhTPP1 halted decline of retinal mixed rod and cone responses in CLN2-affected dogs. Intravitreal injections #1 and #2 were given within 1 week following the Baseline #1 and #2 ERG measurements, respectively. Data from normal (n=7) and CLN2-affected (n=6) untreated dogs are historical data obtained from Dachshunds from the same research colony.

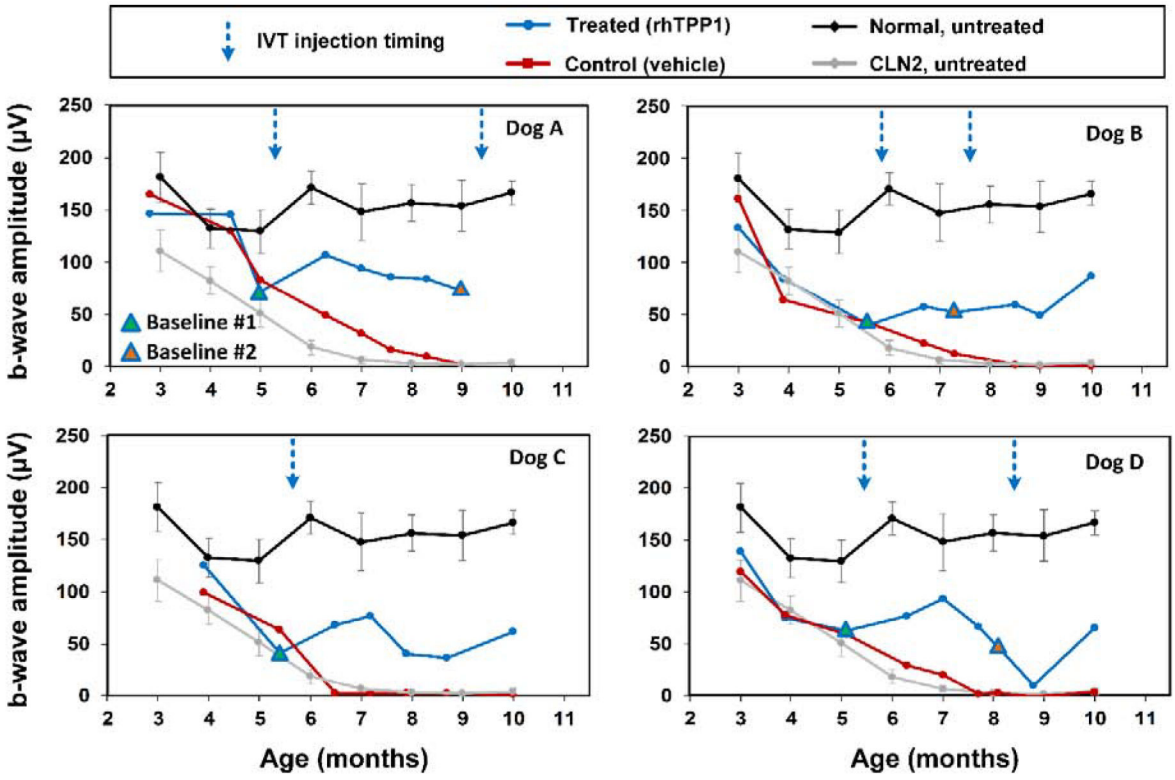

Figure 4.

Post symptomatic intravitreal rhTPP1 halted decline of retinal rod responses in CLN2-affected dogs. Intravitreal injections #1 and #2 were given within 1 week following the Baseline #1 and #2 ERG measurements, respectively. Data from normal (n=7) and CLN2-affected (n=6) untreated dogs are historical data obtained from Dachshunds from the same research colony.

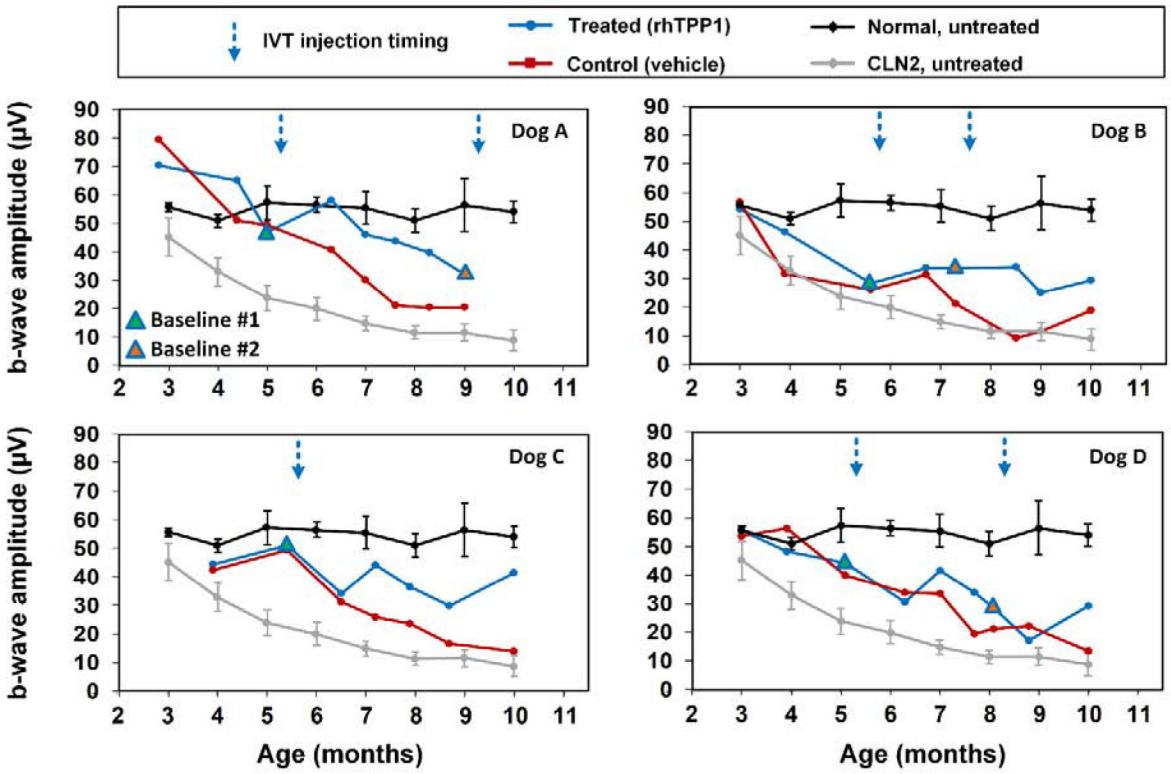

Figure 5.

Post symptomatic intravitreal rhTPP1 halted decline of retinal cone responses in CLN2-affected dogs. Intravitreal injections #1 and #2 were given within 1 week following the Baseline #1 and #2 ERG measurements, respectively. Data from normal (n=7) and CLN2-affected (n=6) untreated dogs are historical data obtained from Dachshunds from the same research colony.

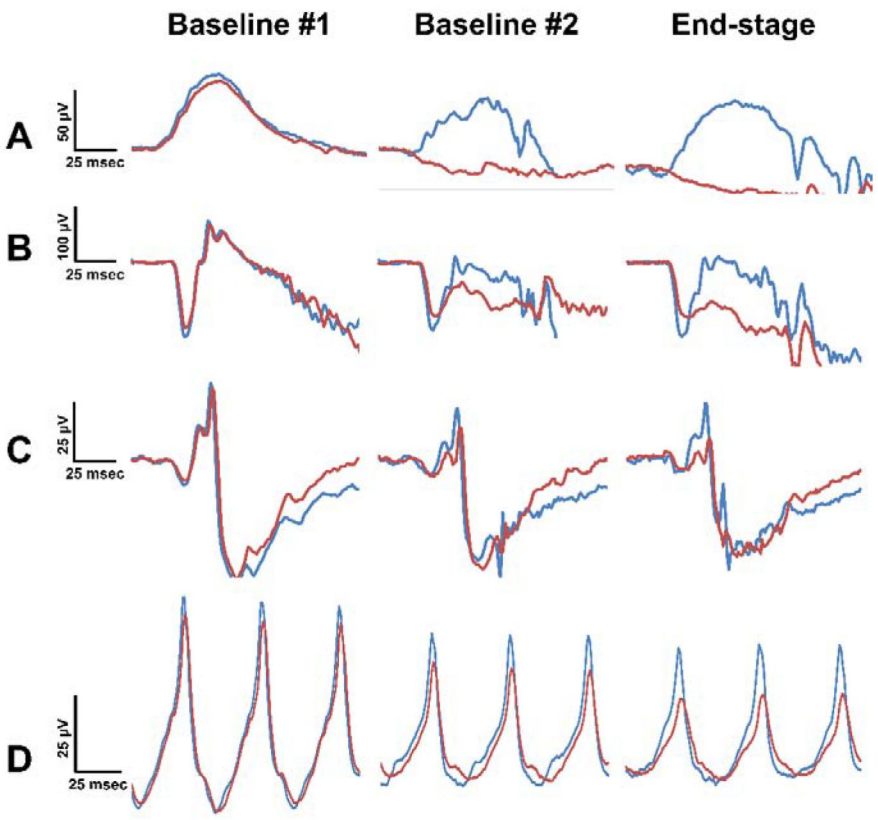

Figure 6.

ERG waveforms from Dog D at ages of 5 months (baseline #1), 8 months (baseline #2), and 10 months (end-stage disease). (A) pure rod, (B) mixed rod and cone, (C) pure cone, and (D) 30 Hz flicker responses all exhibited ERG preservation in the rhTPP1 treated eye relative to the control eye. Baseline #1 and #2 recordings were performed within 1 week prior to intravitreal injections #1 and #2, respectively.

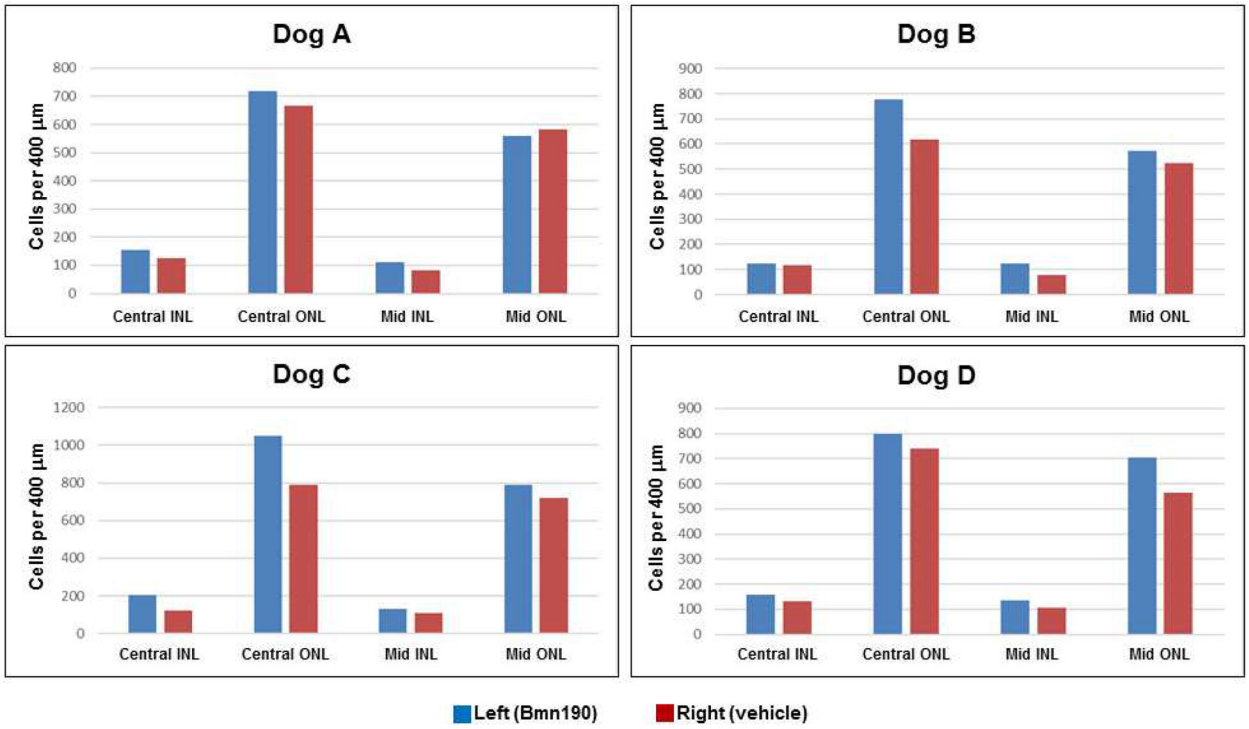

Figure 7.

Numbers of cell nuclei per 400 µm of retinal length in the inner nuclear layer (INL) and outer nuclear (ONL) of the central and superior mid-peripheral regions (regions A1 and B1 indicated in Figure 1 respectively) from the four dogs in the study.

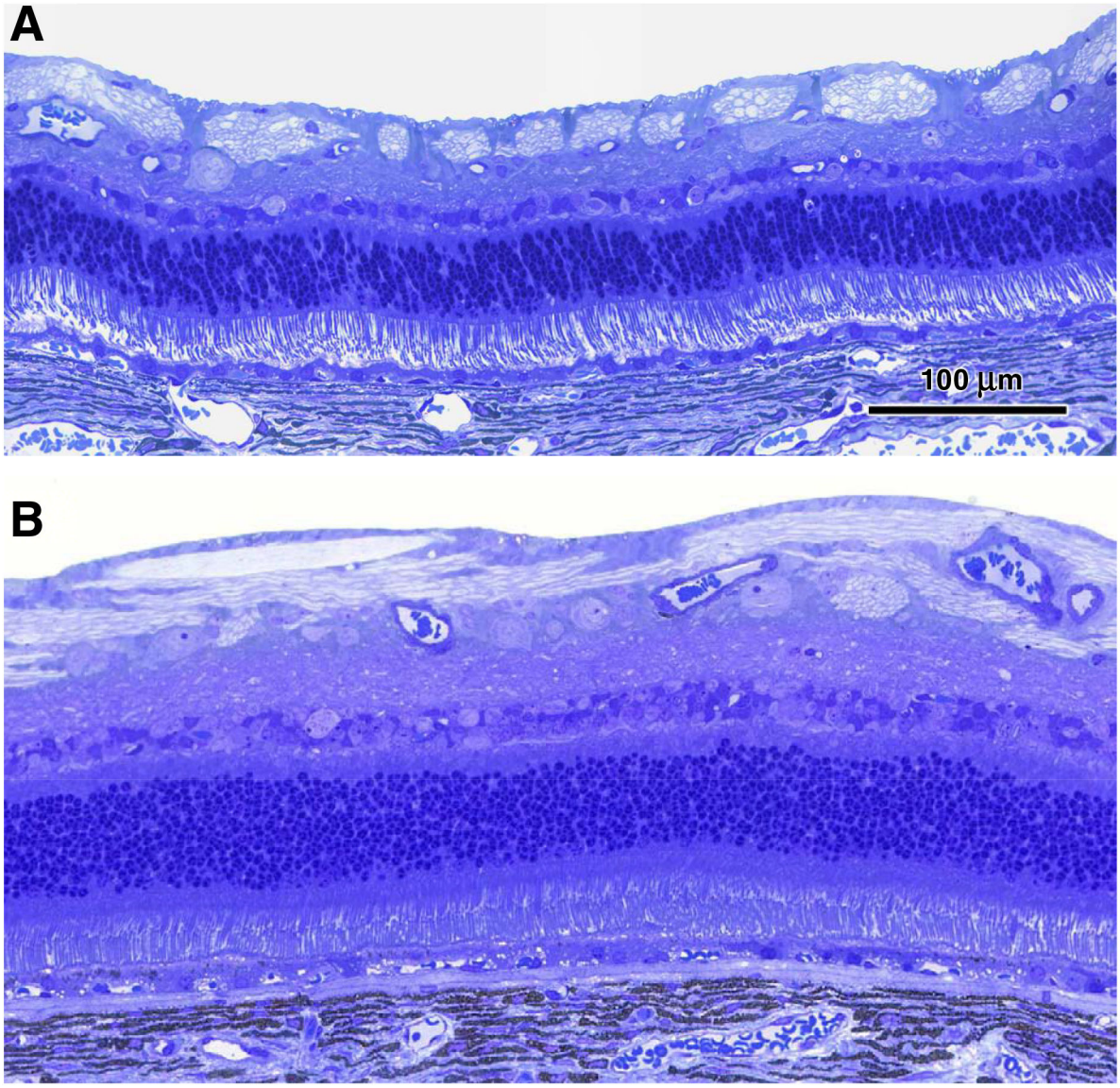

Figure 8.
Representative light micrographs of the central retinas from the vehicle-treated eye (A) and the rhTPP1-treated eye (B) from dog C.

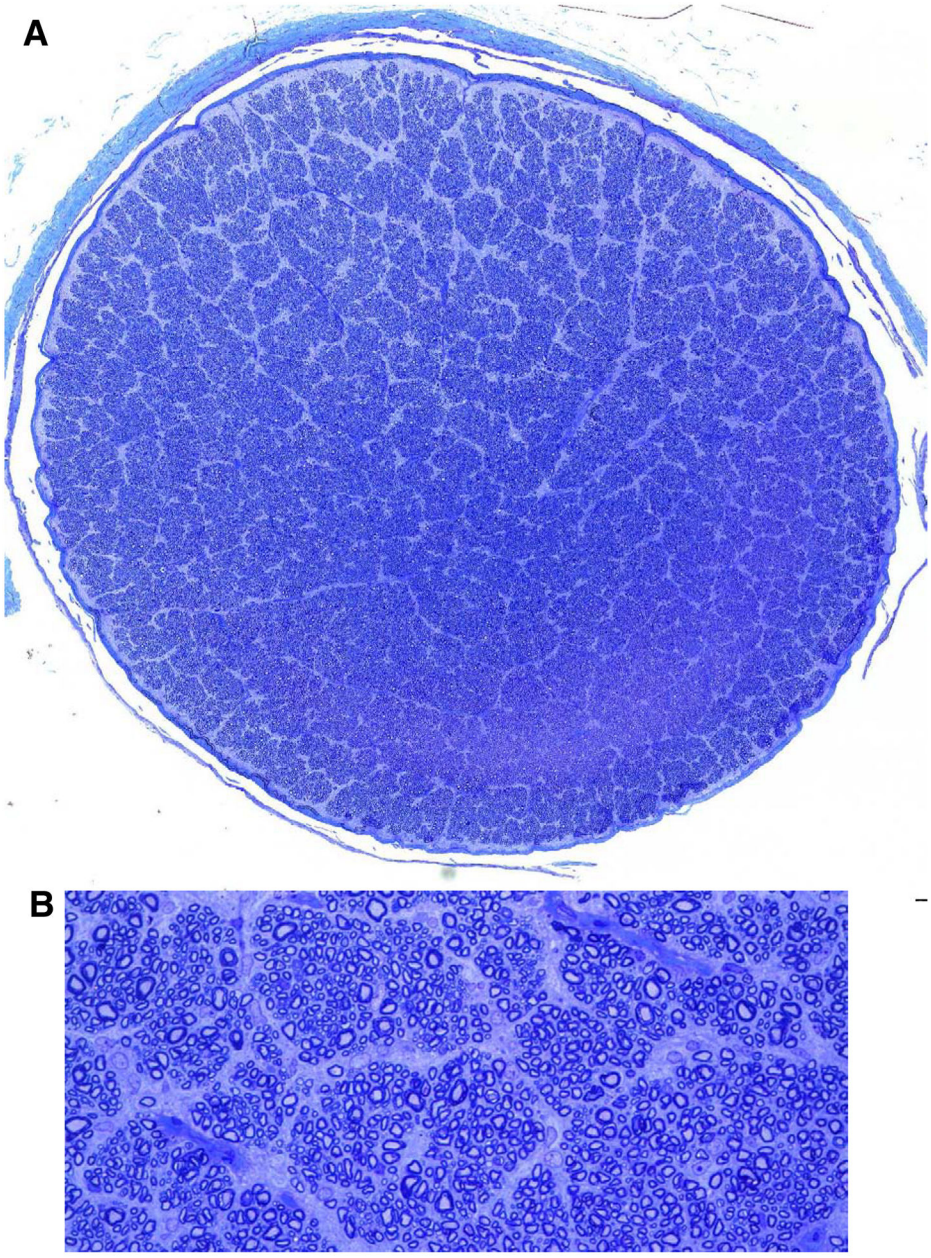

Figure 9.

(A) Light microscopic image of optic nerve cross section from the rhTPP1-treated eye of dog A created by merging high magnification images as described in the methods section. (B) Area of image in (A) enlarged sufficiently to enable counting of individual axons.

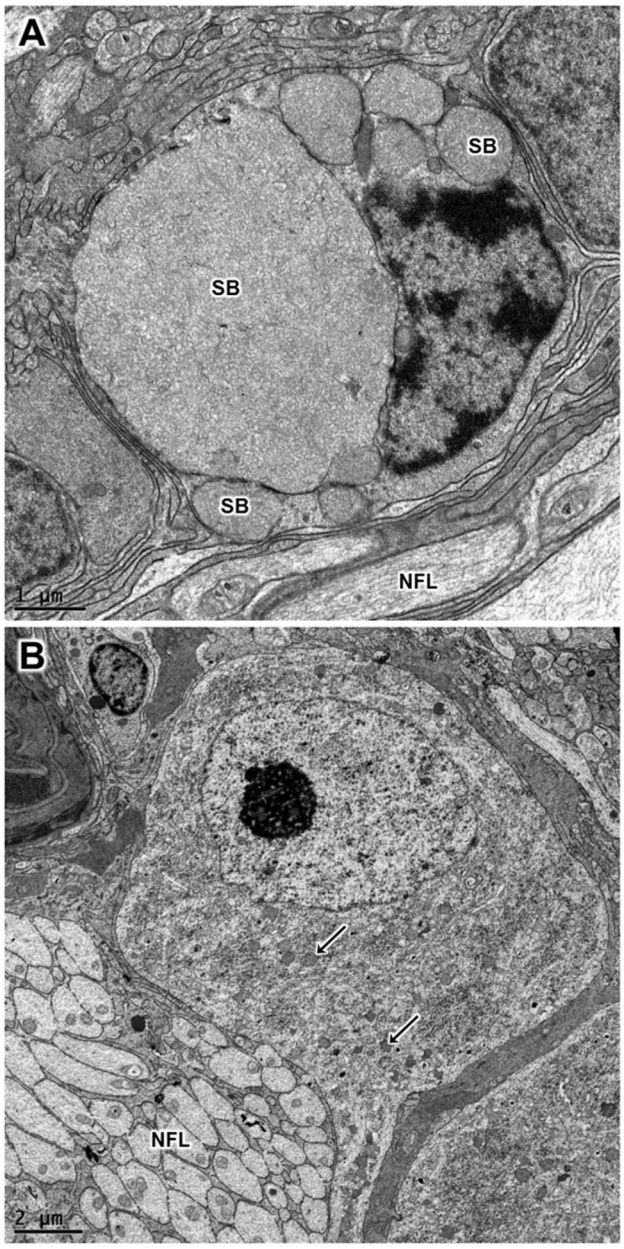

Figure 10.

Electron micrographs of retinal ganglion cells from the vehicle-treated eye (A) and the rhTPP1-treated eye (B) from dog D. The sizes and numbers of ganglion storage bodies (SB) were dramatically lower in the rhTPP1-treated eyes. Representative storage bodies – “SB” in (A) and arrows in B. Nerve fiber layer – “NFL”.

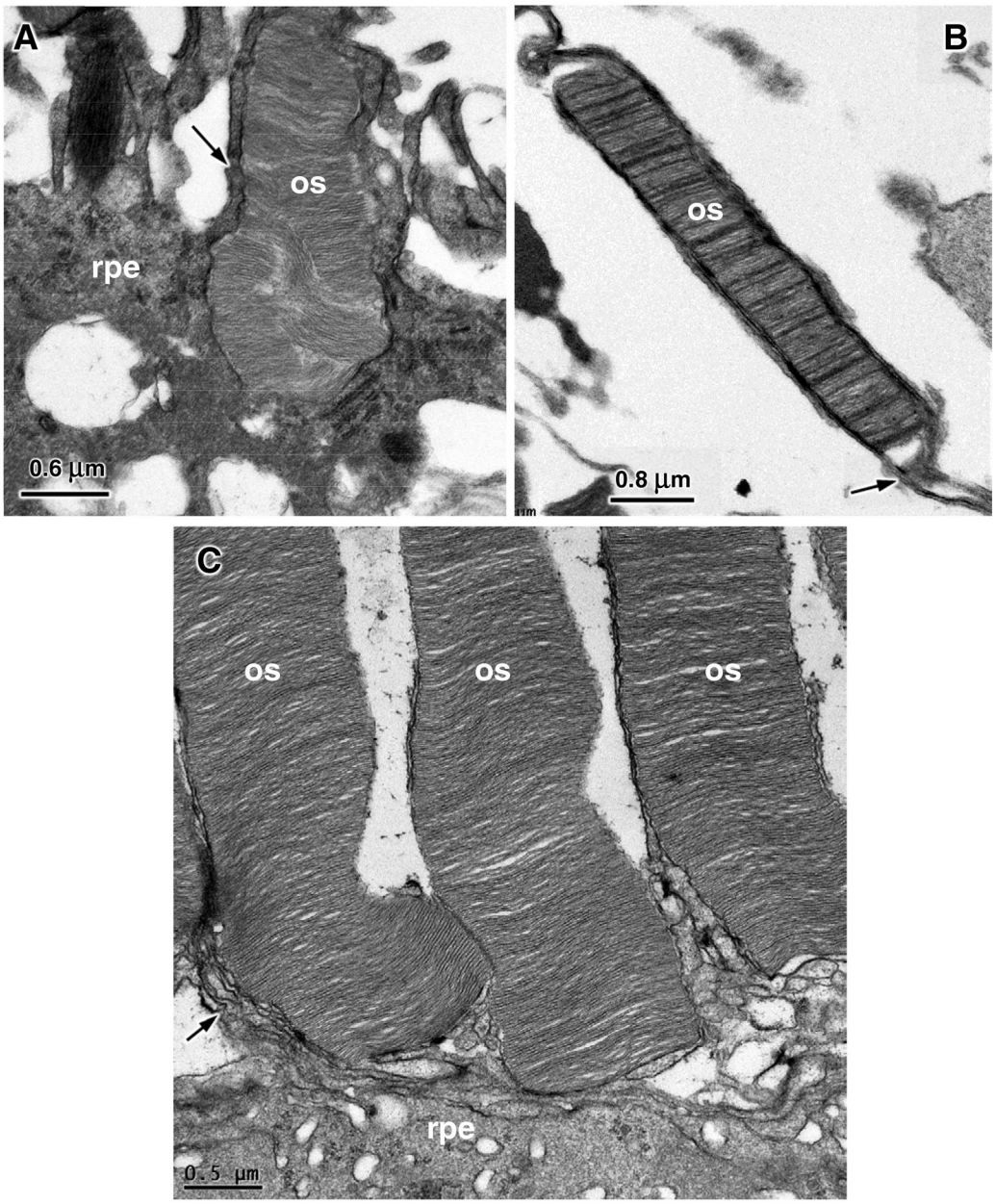

Figure 11.

Electron micrographs of the photoreceptor-retinal pigment epithelium interfaces from the vehicle-treated (A and B) and rhTPP1-treated (C) retinas of Dog D. Rod outer segments (os); retinal pigment epithelium (rpe); rpe apical microvilli (arrows).

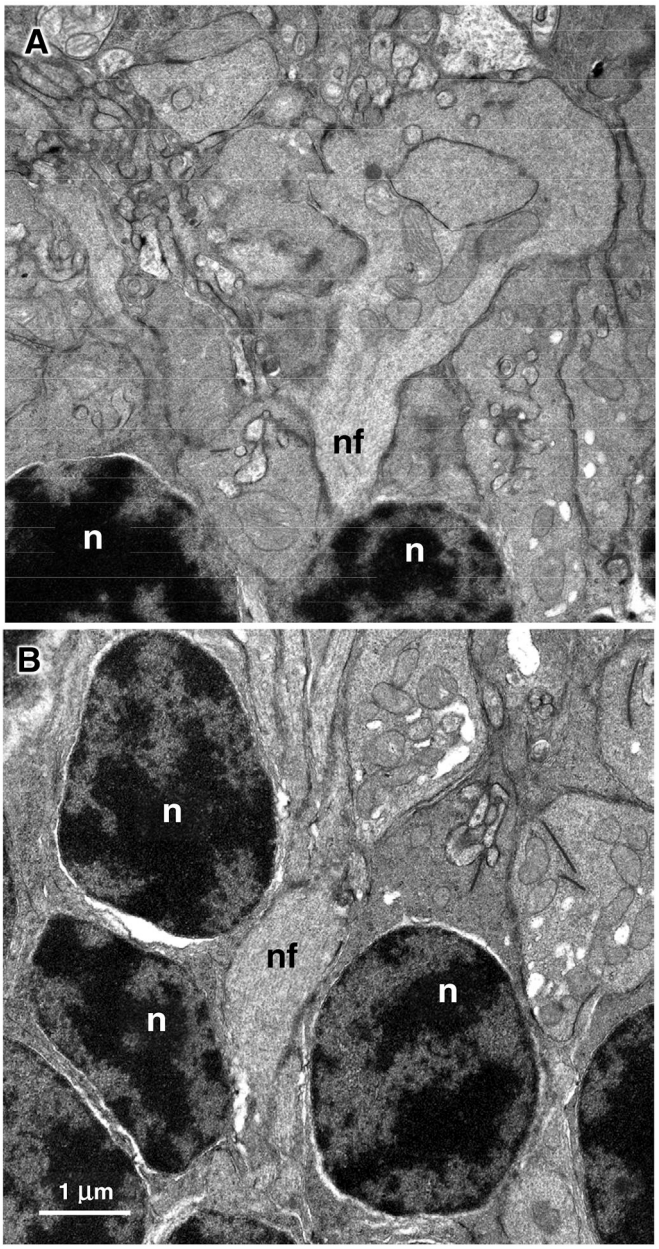

Figure 12.

Electron micrographs of the outer plexiform layer/outer nuclear layer interface of the vehicle-treated (A) and rhTPP1-treated (B) retinas from Dog D. Rod photoreceptor nuclei (n); nerve fibers of bipolar cells (nf). Bar in (B) indicates magnification of both micrographs.

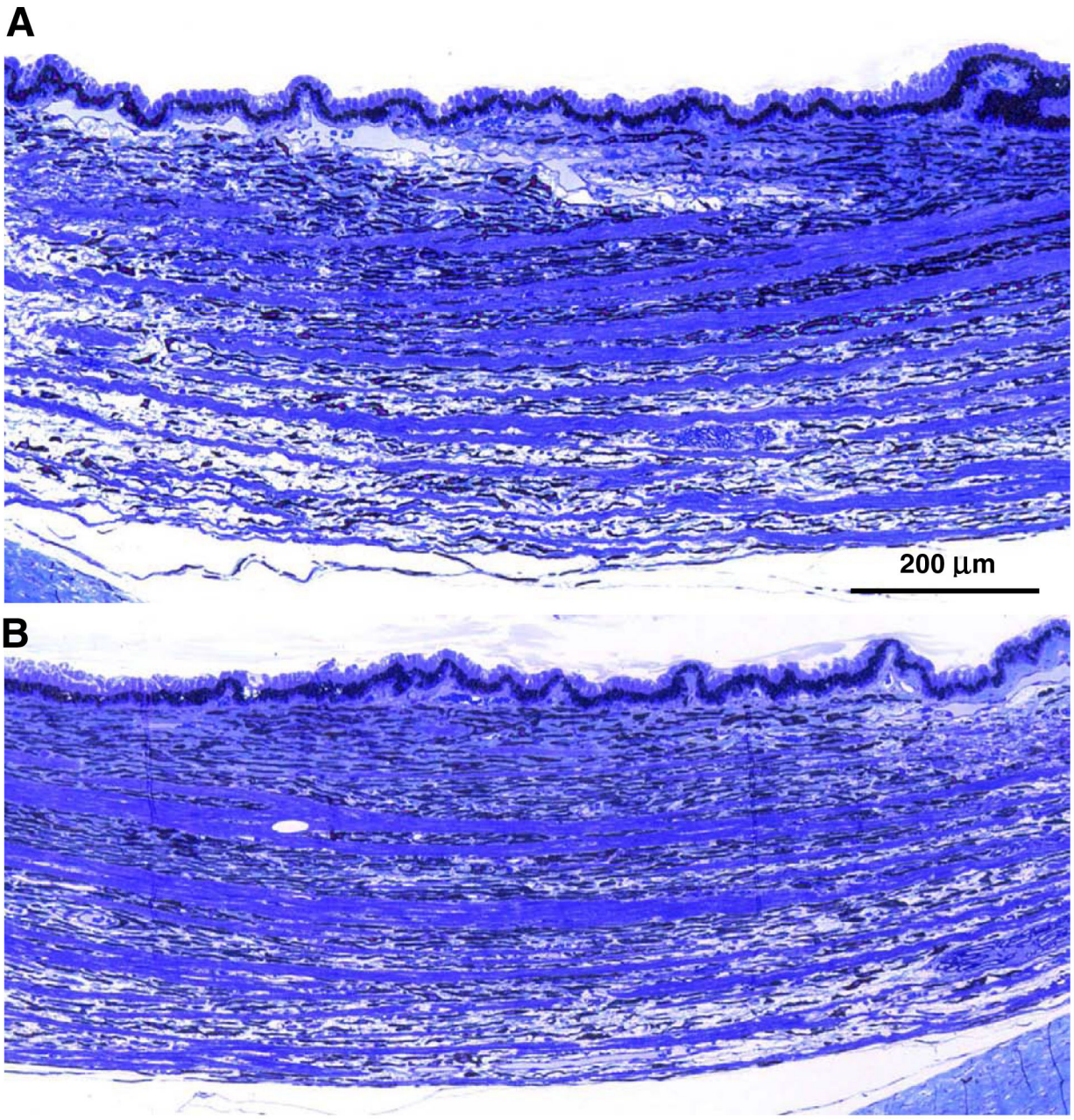

Figure 13.

Light micrographs of the ciliary bodies from the vehicle-treated (A) and BMN-190-treated (B) eyes of dog C euthanized at approximately 10.5 months of age. The ciliary body of the vehicle-treated eye is thicker and includes unstained gaps relative to the more compact ciliary body of the rhTPP1-treated eye.

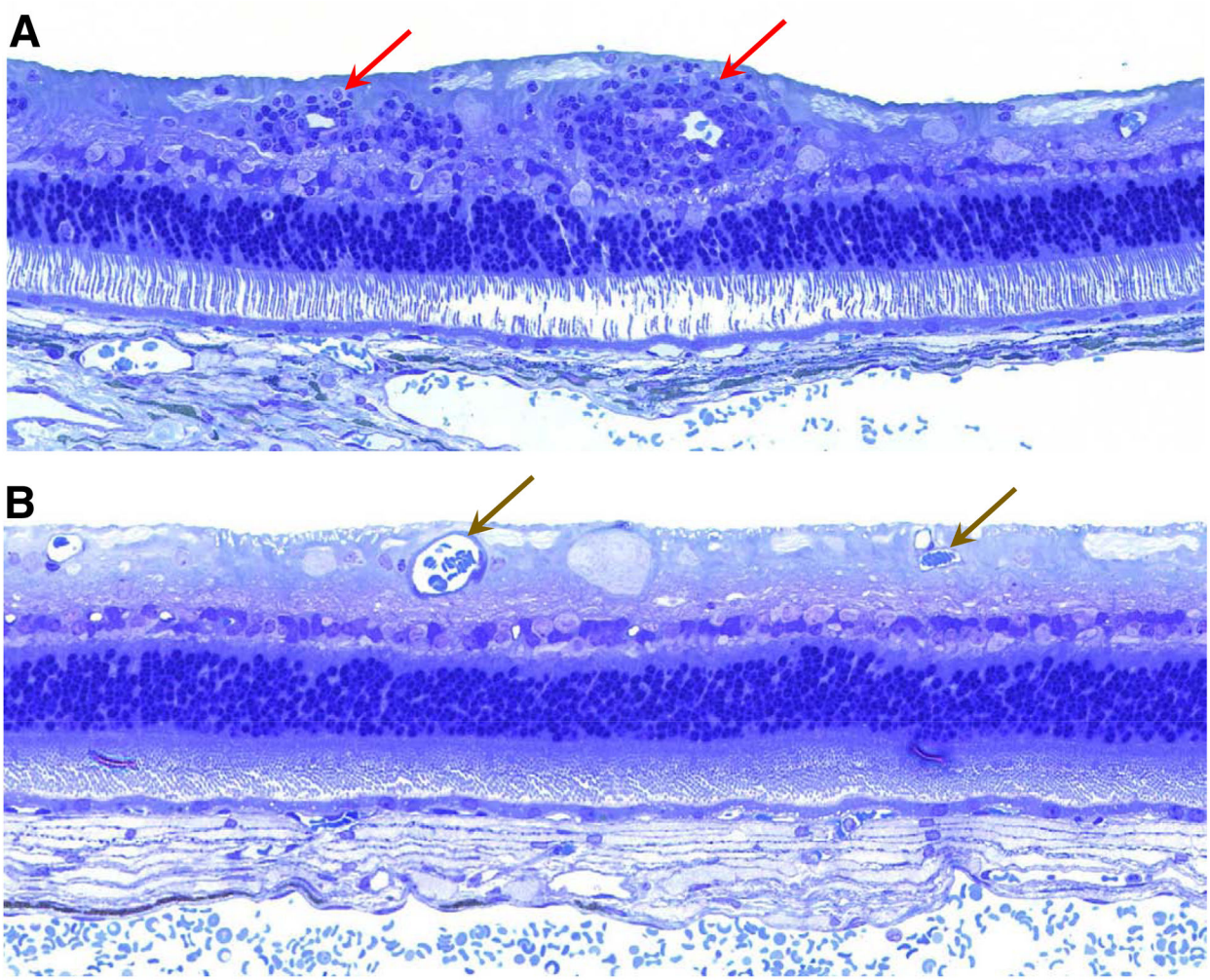

Figure 14.

Light micrographs of sections of the mid-peripheral rhTPP1-treated retinas from dog B (A) and dog C (B). Pronounced perivascular cuffing was present around inner retinal vessels in the central retina of dog B (red arrows), whereas no such cuffing was present around inner retinal vessels (brown arrows) of the retina in dog C.

Table 1:

Individual Animal IVT TPP1 Dosing

Injection	TPP1 Dose (mg)	Age (weeks)			
		Dog A	Dog B	Dog C	Dog D
#1	0.5	23.5	25	25	23.5
#2	0.25	39.5	33.5	--	35.5

Table 2.

Concentrations of TPP1 in the Aqueous and Vitreous Humors of TPP1-Treated Eyes

Dog	Aqueous TPP1 Conc (ng/mL)	Vitreous TPP1 Conc (ng/mL)	Days Since Last Injection
A	15754	62365	1
B	BLQ*	BLQ	67
C	9.23	BLQ	140
D	4.48	BLQ	48

*BLQ – below limit of quantitation; limit of quantitation = 3.91 ng/mL for aqueous humor; 1.95 ng/mL for vitreous humor

Table 3.

Anti-rhTPP1 Titers in Pre-Euthanasia Blood Samples

Dog	Anti-TPP1 Antibody Titer	Days Since Last Injection
A	10	1
B	>163840 *	67
C	640	140
D	>163840 *	48

* Maximum limit of assay.

Table 4.

Numbers of axons in the optic nerves of each dog.

	Number of Optic Nerve Axons		
Dog	**rhTPP1 Treated Eye (T)**	**Vehicle Treated Eye (C)**	**C/T × 100**
A	141,438	125,177	88.5
B	141,074	141,161	100.1
C	139,596	133,182	95.4
D	153,289	136,057	88.8

Table 5.

Effect of rhTPP1 treatment on storage body content of retinal ganglion cells

	Storage Body Content (% cytoplasmic area occupied by storage bodies) -- Mean + SE*		
Dog	**rhTPP1 Treated Eye**	**Vehicle Treated Eye**	**P value**
A	2.1 ± 0.3	26.8 ± 3.5	<0.001
B	6.2 ± 1.8	26.0 ± 5.8	0.002
C	2.7 ±0.7	29.5 ±2.3	<0.001
D	2.7 ±0.7	34.9 ± 7.9	<0.001

Table 6:

Perivascular Cuffing Around Inner Retina Vessels

	Dog A		Dog B		Dog C		Dog D	
	Age (Weeks)	**rhTPP1 Dose (mg)**	**Age (Weeks)**	**rhTPP1 Dose (mg)**	**Age (Weeks)**	**rhTPP1 Dose (mg)**	**Age (Weeks)**	**rhTPP1 Dose (mg)**
	25	0.5	25	0.5	25	0.5	25	0.5
	39.5	0.25	33.5	0.25			35.5	0.25
Euthanized (age, weeks)	40		45		44.5		42	
Perivascular Cuffing	Absent		Present		Absent		Present	